Artificial Neural Network Prediction of Weld Geometry Performed Using GMAW with Alternating Shielding Gases

A sensitivity analysis showed travel speed is the most influential input parameter when predicting weld geometries

BY S. W. CAMPBELL, A. M. GALLOWAY, AND N. A. McPHERSON

ABSTRACT

An artificial neural network (ANN) model has been applied to the prediction of key weld geometries produced using gas metal arc welding (GMAW) with alternating shielding gases. This is a recently developed method of supplying two individual shielding gases to the weld area in which the gases are discretely supplied at a given frequency. The model can be used to predict the penetration, leg length, and effective throat thickness for a given set of weld parameters and alternating shielding gas frequency.

A comparison of the experimental and predicted geometries matched closely and demonstrates the effectiveness of this software approach in predicting weld outputs. The model has shown that the application of alternating shielding gases increases the penetration and effective throat thickness of a fillet weld while the leg length is reduced.

A sensitivity analysis was performed that showed travel speed is the most influential input parameter when predicting weld geometries. This is to be expected for any given welding setup due to the influence of the travel speed on the heat input. The sensitivity analysis also showed that the shielding gas configuration had the lowest influence on the output of the model. The output from the model has demonstrated that the use of alternating shielding gases during GMAW results in a step change in the weld metal geometry. This suggests that, in the case of alternating shielding gases, an increased travel speed is required to produce a similar weld geometry to that of the conventional Ar/20%CO_2 technique.

Introduction

Shielding gases are fundamental to the operation of the gas metal arc welding (GMAW) process and there are a number commonly used, each with its own specific properties, i.e., ionization potential, which creates unique arc characteristics (Refs. 1–7). Shielding gases are also commonly used in a variety of premixed combinations of two or more gases in order to take advantage of the beneficial properties of each gas (Refs. 8, 9). Recently, however, there has been some positive research (Refs. 1–4) into the effects of alternating shielding gases in both GMAW and, to a lesser extent, gas tungsten arc welding. This method involves discretely supplying two different shielding gases, each with a duty cycle of 50%; i.e., while one gas is flowing the other is not, which results in a continuous shield with varying properties. These studies have shown beneficial results including an increased travel speed, reduced porosity, and increased strength. For example, Campbell et al. (Ref. 1) reported the use of alternating shielding gases can reduce the overall weld cost by approximately 17% while also considerably reducing distortion. Chang (Ref. 2) reported the use of alternating shielding gases created beneficial effects on the weld pool and, as shown in Fig. 1 (Ref. 3), different flow vectors were created in the weld pool for different gases used. However, when alternating between shielding gases, complex flow patterns were created that caused a dynamic action in the weld pool and this is known to be a result of the fluctuation between these individual shielding gas flow vectors. The dynamic nature of the shielding gas delivery is known to be influenced by factors such as (a) arc pressure variation, (b) variation in weld pool fluidity, and (c) arc pressure peaking.

As several industry sectors (e.g., shipbuilding and road transportation) move toward thinner and stronger materials in order to reduce the overall mass of the structure (Refs. 10, 11), it is widely recognized that these thinner materials are more susceptible to distortion induced by the heat input generated by the welding processes used during fabrication. Distortion is a result of the nonuniform expansion and contraction of the weld material due to the heating and cooling cycle (Ref. 11) and although computational models can be used to help predict the magnitude of weld-induced distortion (Ref. 12), as a result of the number of variables involved (Ref. 13) including material properties, welding procedure, structural design, and manufacturing procedure (each of which have numerous sub variables) results in such models being specific to the data used in the model generation. However, the effort required to rectify the distortion from the steel structure is highly resource intensive. For that reason it is beneficial to eliminate as much distortion at the source as possible and this is largely achievable through good practices, mainly related to reducing the heat going into the steel structure and the concentration of heat in specific areas. Further, there is an increasing demand for quality prediction in today's ever-increasing automated soci-

KEYWORDS

Gas Metal Arc Welding
Artificial Neural Networks
Alternating Shielding Gases

S. W. CAMPBELL and A. M. GALLOWAY are with Department of Mechanical Engineering, University of Strathclyde, Glasgow, Scotland. N. A. McPHERSON is with BAE Systems Surface Ships Ltd., Glasgow, Scotland.

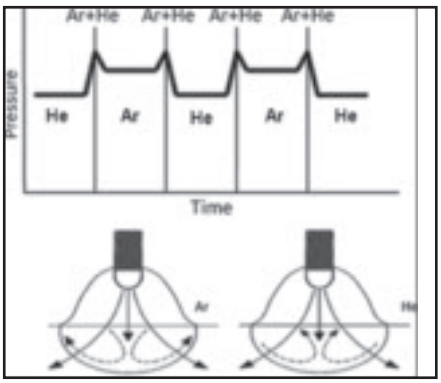

Fig. 1 — Arc pressure and fluid flow vectors (Ref. 3).

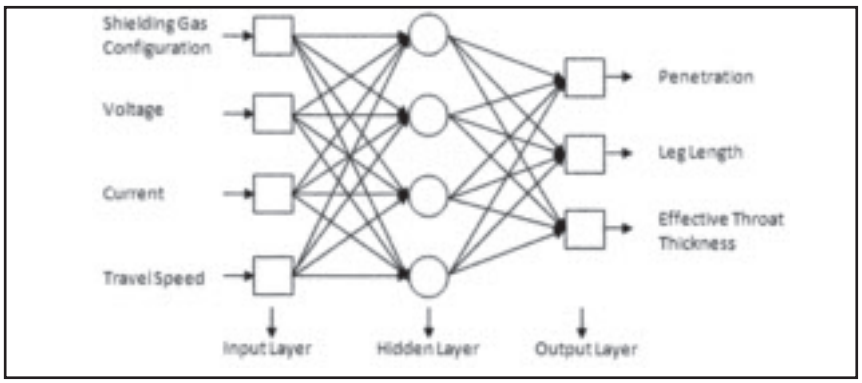

Fig. 2 — Multilayer perceptron architecture with one hidden layer.

ety, and it is imperative that there is a high level of consistency in the process in order to satisfy this demand.

While the external fillet weld geometry can be measured, there is no way of knowing the penetration of the weld without the aid of nondestructive testing although improved accuracy may be obtained by sectioning and polishing the sample. As both of these geometry details are important in terms of weld integrity, it is clear that an optimized approach needs to be taken such that the maximum penetration and effective throat are deposited to satisfy the structural integrity demands with the converse being the case in terms of minimizing the weld heat input and final distortion. Hence, in an attempt to achieve the optimum weld geometry conditions, the implementation of various model simulation environment software, such as artificial neural networking (ANN), offers considerable predictive strength to this optimization approach.

Artificial neural networks are mathematical or computational models that are able to capture and represent complex input-output relationships. They are distributed, adaptive, generally nonlinear learning machines built from many different processing elements (PEs) (Ref. 14). McCulloch and Pitts (Ref. 15) developed the first neural networks in 1943 based upon their understanding of neurology; this operated using simple and/or logic functions and made several assumptions as to the operation of neurons. Major advances were made around 1960 when Rosenblatt (Ref. 16) designed and developed the perceptron, which was constructed by multiple layers and allowed the system to learn to associate a given input to an output. Around the same time, Widrow and Hoff (Ref. 17) developed the ADALINE (ADAptive LINear Element) system, an analogue electronic device that operated on the Least Mean Square (LMS) learning rule. Werbos (Ref. 18) developed the backpropagation learning method in the early 1970s and although this learning method took a number of years to gain popularity, it is now probably the best known and applied learning method used today. The interconnectivity of the PEs defines the topology of the network. There are three main network topologies commonly implemented:

- Multilayer Perceptron (MLP)
- Generalized Feed-Forward (GFF)
- Modular Feed-Forward (MFF)

Neural networks can be used to predict any process as long as sufficient data are generated to accurately train and validate the model. The GMAW process is extremely complex and involves the interaction of several nonlinear welding variables. Artificial neural networks have the ability to develop patterns and detect subtle link/trends that are too complex to be observed via other techniques, therefore allowing for the strong indicators of new situations of interest. In addition, other computational modeling environments are unidirectional, i.e., calculate an output for a given set of input variables, and often require extensive computational power to process complex models whereas ANNs are bidirectional and have the ability to predict the input variables required to produce a given output. The ANNs can, therefore, be employed to accurately predict mechanical properties and other important weld characteristics without the need for destructive testing, while precise models will provide confidence in the welds produced.

The basic architecture of an ANN is shown in Fig. 2 and consists of interconnected processing elements in the different layers of the system:

An input layer — represents the raw data that are fed into the system

One or more hidden layers — the output of which is determined by the activities of the inputs and the weights of the connections

An output layer — conveys the signals to the environment and is dependent upon the processes and weights of the hidden units.

This type of computational model can be effectively applied to the welding process where the input layer consists of the welding parameters and the output layer is made up of the weld geometry, mechanical properties, and other factors as a consequence of the input parameters.

Artificial neural networks were first applied to the welding process around the early 1980s (Refs. 19, 20). Since then they have been used extensively in the prediction of weld characteristics such as mechanical properties (Refs. 21–25) and have been shown to be fairly accurate in determining tensile strength, hardness, elongation, and impact energy. They have been used to determine the weld quality (Ref. 26) based upon differing input settings including current, voltage, and gas compositions. Artificial neural networks have also been implemented for the prediction of weld-induced deformation (Refs. 27, 28) and weld geometry (Refs. 29–31). Although ANNs have previously been used for the prediction of various welding parameters, there have been no publications for the prediction of welding parameters while implementing this novel technique of alternately supplying shielding gases. Further information on the historical development of ANNs toward welding processes is reported elsewhere (Refs. 32, 33).

Experimental Setup

The material used throughout was 6-mm-thick DH36 grade steel in the form of 60-mm-wide bar with a typical chemical composition shown in Table 1. The bars were tacked together in the form of an inverted 'T' as shown in Fig. 3.

The average welding parameters are shown in Tables 2A and 2B. The gas flow was controlled using an electronic control unit (Fig. 4), which allowed the alternating frequency to be accurately set prior to welding while implementing an oscilloscope for validation. The basis of the unit was two timing circuits (one for each gas)

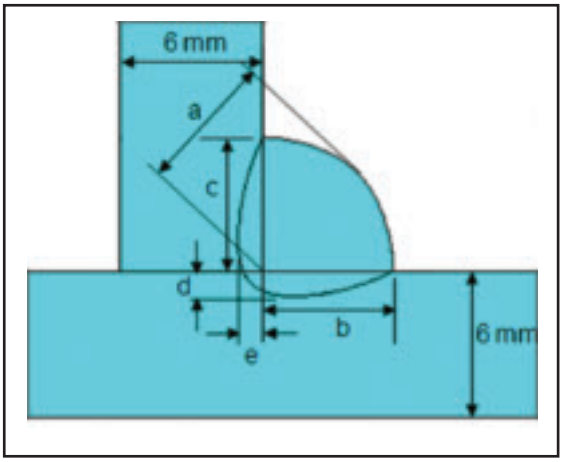

Fig. 3 — Weld detail showing geometries measured.

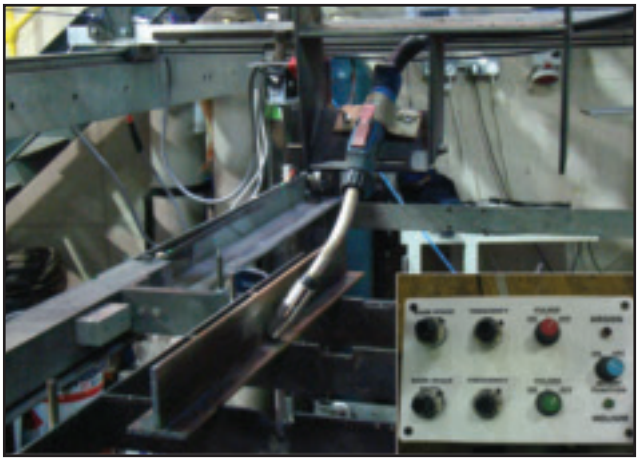

Fig. 4 — Automatic welding rig (Insert: gas control unit).

that generated a continuous square wave at a specified frequency. The output from the timing circuits was then used to control the current supply to the solenoid valves in order to regulate the flow of each gas. The unit incorporated an invert function to supply opposite signals to each valve for alternation precision, thus generating a pressure-time graph comparable to that shown in Fig. 1. It is important to recognize that although the alternating frequency is a variable during experimentation, each gas is supplied for 50% of the time regardless of the frequency. Since the flow rate of each gas was preset at 15 L/min (when flowing continuously), the overall gas consumption remained 15 L/min independent of the frequency. At present, the device used for alternating the shielding gases is an experimental unit that is not currently commercially available. However, the unit is a simple setup that was minimal in cost to generate. The potential savings and benefits (Ref. 1) of the system are likely to substantially outweigh any modest capital investment required to implement the technology on a commercial scale.

Table 1 — Chemical Composition of DH36 Steel (trace indicates nondeliberate additions)

Element	Chemical Compostion (wt-%)
Carbon	0.15
Silicon	0.35
Manganese	1.38
Phosphorus	0.013
Sulfur	0.012
Chromium	0.017 (trace)
Molybdenum	0.001 (trace)
Nickel	0.018 (trace)
Aluminum	0.026
Copper	0.01 (trace)
Niobium	0.025
Nitrogen	0.003

There are various filler materials used in industry depending upon the application and the ability of each to be used in a particular weld position including solid wire, metal cored wire, and flux cored wire. One-mm metal cored wire (EN 758: T46 4 M M 1 H5), which has a typical all-weld-metal chemical composition as shown in Table 3, was used throughout experimentation with a constant feed speed of 90 mm/s.

All experimental welds were deposited on an automatic welding rig where the plate, held rigid, moved at a preset speed under a fixed welding nozzle as shown in Fig. 4. The nozzle used was adapted so as to allow the helium to be directly supplied to the welding zone — Fig. 5. In each case the welds were produced using a torch preset at a 45-deg angle and fixed in position.

A precalibrated, portable arc monitoring system (PAMS) was used throughout to accurately obtain the welding arc voltage and current. The on-board A-D converter of the PAMS unit has a 14-bit resolution that results in the voltage being accurate to approximately 0.012 V and the current to approximately 0.12 A. The sample frequency of the unit is 5 kHz and will therefore accurately represent the average parameters even when alternating between gases since the sample frequency (5 kHz) is very much greater than the alternating frequency (2–8 Hz).

Model Development

The software implemented for this study was *NeuroSolutions*, which had previously been used successfully for the prediction of weld geometries (Ref. 31) and distortion (Ref. 27). A total of 45 samples was produced (9 for each gas configuration), a hold-out method was used throughout the model generation process, in which 40 samples were used for the training of the model while the remaining 5 (one for each gas configuration) for testing. These data are displayed in Table 2A. The same five test data sets were used throughout in order to produce a direct comparison on the accuracy of the model using each of the topologies. Throughout model generation, each model was run three times and the average error taken. This was done since the same topology with the same training data can produce so many different sets of final weights. There are three main reasons behind this:

- There are many symmetries in the input-output mapping created by the MLP.
- There is no guarantee that the problem has a single solution.
- The final weights are obtained in an iterative fashion from random initial values.

The following network topologies were considered:

- Multilayer Perceptron (MLP)
- Generalized Feed-Forward (GFF)
- Modular Feed-Forward (MFF)

Mathematically, the output from each of the models is the same and can be represented as shown in Equation 1:

$$O = \sum_{n=1}^{n} I_n * w_n \qquad (1)$$

where O is the output, I_n is the n^{th} input sample, w_n is the weight of the n^{th} sample, and n is the number of samples.

It was found that although the MLP topology produced a higher mean square error than the GFF and MFF topologies, when comparing the percentage errors of the test data sets it was found that the MLP topology produced the lowest error and was therefore selected.

There is an optimum number of iterations for training the model and, consequently, the number of learning iterations had to be determined. The model was

Table 2A — Training/Testing Weld Data

	Weld Parameters			Weld Outputs		
Shielding Gas Configuration	Voltage (V)	Current (I)	Travel Speed (mm/s)	Penetration (mm)	Leg Length (mm)	Effective Throat (mm)
$Ar/20\%CO_2$	21.7	158	2.0	1.168	6.739	4.626
$Ar/20\%CO_2$	23.6	157	2.0	1.471	6.541	4.710
$Ar/20\%CO_2$	26.0	157	2.0	0.992	7.628	4.943
$Ar/20\%CO_2$	22.0	151	2.5	1.483	6.249	4.626
$Ar/20\%CO_2$	23.9	154	2.5	1.044	6.687	4.182
$Ar/20\%CO_2$	26.1	157	2.5	1.070	6.894	4.357
$Ar/20\%CO_2$	21.9	152	3.0	1.078	5.300	3.298
$Ar/20\%CO_2$	23.8	158	3.0	1.391	6.371	3.916
$Ar/20\%CO_2$	26.1	158	3.0	1.136	6.506	4.228
Alternating @ 2 Hz	21.8	153	2.0	1.229	6.803	5.637
Alternating @ 2 Hz	23.4	156	2.0	1.421	6.977	4.646
Alternating @ 2 Hz	26.4	159	2.0	1.365	7.171	4.616
Alternating @ 2 Hz	22.0	157	2.5	1.020	6.559	4.964
Alternating @ 2 Hz	23.7	156	2.5	1.269	5.789	3.807
Alternating @ 2 Hz	25.8	159	2.5	1.116	7.634	5.236
Alternating @ 2 Hz	21.9	152	3.0	1.107	5.365	4.748
Alternating @ 2 Hz	23.4	155	3.0	1.426	5.319	4.556
Alternating @ 2 Hz	26.2	154	3.0	1.342	5.498	4.200
Alternating @ 4 Hz	21.6	150	2.0	1.148	6.913	5.752
Alternating @ 4 Hz	23.9	155	2.0	1.494	6.680	5.091
Alternating @ 4 Hz	25.8	156	2.0	1.499	6.582	4.879
Alternating @ 4 Hz	21.7	157	2.5	1.277	6.196	4.818
Alternating @ 4 Hz	23.7	155	2.5	1.315	6.467	4.869
Alternating @ 4 Hz	25.6	157	2.5	1.371	6.207	4.032
Alternating @ 4 Hz	21.9	154	3.0	1.235	5.727	4.798
Alternating @ 4 Hz	23.8	159	3.0	1.581	4.969	3.333
Alternating @ 4 Hz	26.1	156	3.0	1.290	5.699	4.407
Alternating @ 6 Hz	21.7	154	2.0	1.338	6.416	5.680
Alternating @ 6 Hz	23.5	159	2.0	1.690	6.352	4.855
Alternating @ 6 Hz	25.6	159	2.0	1.347	7.069	4.563
Alternating @ 6 Hz	22.0	152	2.5	1.172	6.239	4.975
Alternating @ 6 Hz	24.3	153	2.5	1.577	5.926	4.044
Alternating @ 6 Hz	25.5	156	2.5	1.198	6.303	3.928
Alternating @ 6 Hz	21.8	156	3.0	1.069	5.133	3.812
Alternating @ 6 Hz	24.0	151	3.0	1.216	5.703	3.679
Alternating @ 6 Hz	25.6	156	3.0	1.702	5.856	3.609
Alternating @ 8 Hz	21.7	155	2.0	0.915	7.326	5.589
Alternating @ 8 Hz	24.0	158	2.0	1.039	7.279	4.475
Alternating @ 8 Hz	25.9	158	2.0	1.522	7.368	4.617
Alternating @ 8 Hz	21.9	154	2.5	1.141	6.459	4.664
Alternating @ 8 Hz	23.9	153	2.5	1.244	6.490	4.093
Alternating @ 8 Hz	26.0	155	2.5	1.415	6.901	4.265
Alternating @ 8 Hz	22.2	153	3.0	1.503	5.364	4.449
Alternating @ 8 Hz	24.0	157	3.0	1.263	5.370	4.014
Alternating @ 8 Hz	26.0	155	3.0	1.711	5.886	3.940

Table 2B — Validation Weld Data

	Weld Parameters			Weld Outputs		
Shielding Gas Configuration	Voltage (V)	Current (I)	Travel Speed (mm/s)	Penetration (mm)	Leg Length (mm)	Effective Throat (mm)
Alternating @ 5 Hz	21.7	153	2.0	1.288	6.835	5.675
Alternating @ 5 Hz	23.8	156	2.0	1.534	6.922	4.923
Alternating @ 5 Hz	25.8	157	2.0	1.421	7.052	4.652
Alternating @ 5 Hz	21.9	157	2.5	1.201	6.177	4.955
Alternating @ 5 Hz	24.0	154	2.5	1.363	6.431	4.366
Alternating @ 5 Hz	26.1	155	2.5	1.315	6.661	4.211
Alternating @ 5 Hz	22.1	154	3.0	1.218	5.295	4.352
Alternating @ 5 Hz	23.9	157	3.0	1.341	5.480	3.934
Alternating @ 5 Hz	25.8	156	3.0	1.523	5.794	3.892

Fig. 5 — Welding torch showing adapted nozzle.

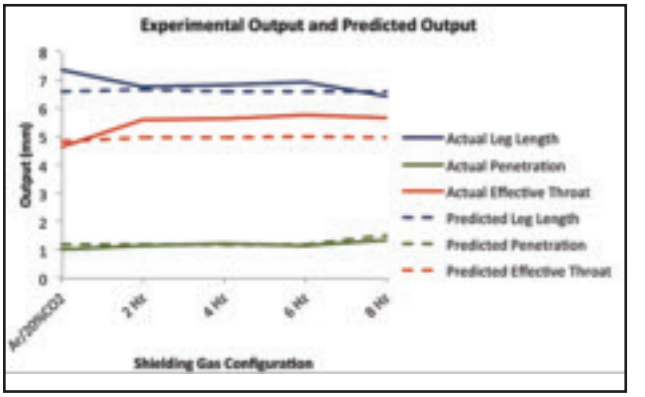

Fig. 6 — Comparison of experimental and predicted geometries.

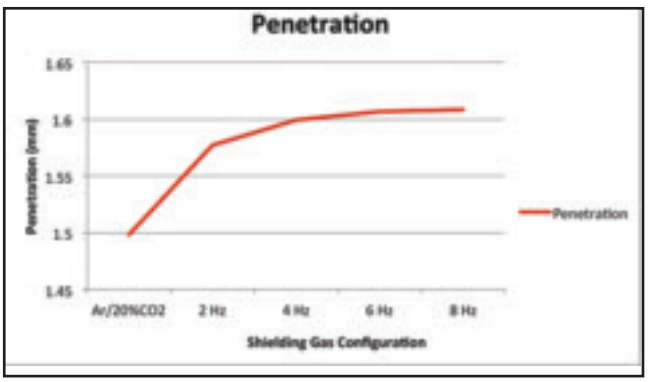

Fig. 7 — Effect of shielding gas configuration on predicted penetration.

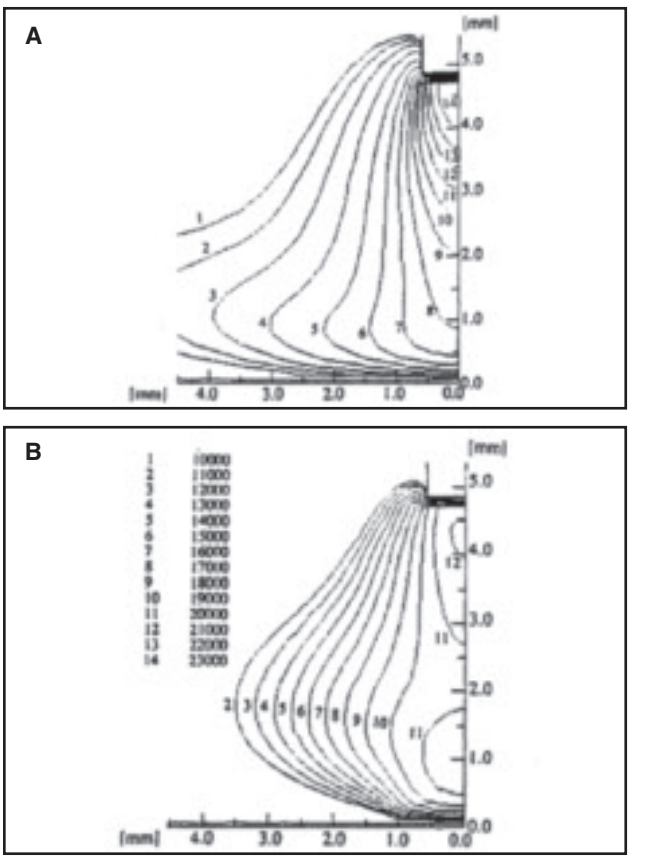

Fig. 8 — Temperature contours at a 200-A welding current (Ref. 25) for the following: A — Argon; B — helium.

Table 3 — Chemical Composition of Welding Wire

Element	Chemical Compostion (wt-%)
Carbon	0.05
Silicon	0.5
Manganese	1.3
Phosphorous	<0.015
Sulphur	<0.015

trained using between 4000 and 20,000 iterations, with 8000 iterations producing the lowest percentage error and, therefore, the most accurate approximation. Contrary to what would be logically expected, the neural network can become overtrained and the percentage error actually increases above 8000 iterations (Ref. 14).

The number of hidden layers of processing elements (PEs) that are not connected directly to the external world was established. There are two extreme cases for the number of hidden layers: either the network has too many PEs to do the job, or it has too few. The model was run with 1–5 hidden layers; it was found that the 1 hidden layer model returned the lowest percentage error of the test data.

Momentum learning was then applied to the model, which is an improvement to the straight gradient-descent search in the sense that a memory term is used to speed up and stabilize convergence. The use of a momentum coefficient helps stop the learning process getting stuck in a local minimum or flat spot. In momentum learning, the equation to update the weights becomes Equation 2.

$$w_{ij}(n+1) = w_{ij}(n) + \eta\delta_i(n)x_j(n) + \alpha\left(w_{ij}(n) - w_{ij}(n-1)\right) \quad (2)$$

where w_{ij} is the weight that connects the i^{th} PE to the j^{th} PE, n is the iteration number, η is the step size, δ_i is the computed error at the i^{th} PE, x_j is the flow of activations at the j^{th} PE, and α is the momentum constant.

The use of momentum learning results in the weighting changing proportionally to how much they are updated in the previous iteration. The momentum constant can have a value of between 0 and 1. It was determined that a value of 0.7 produced the most accurate model.

The final stage in the model development is specifying when the weights are updated. Online learning updates the weights after the presentation of each data set. In contrast, batch learning updates the weights

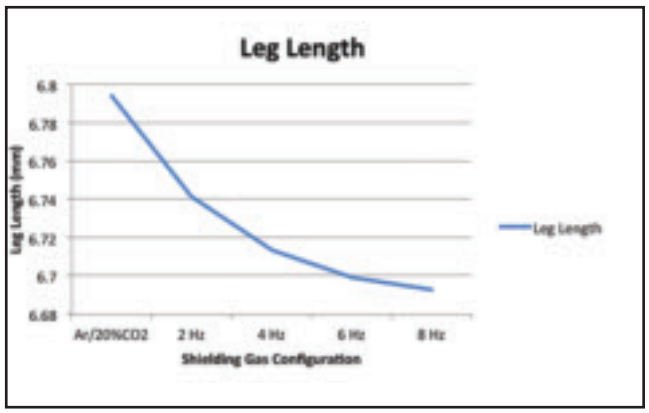

Fig. 9 — Effect of shielding gas configuration on predicted leg length.

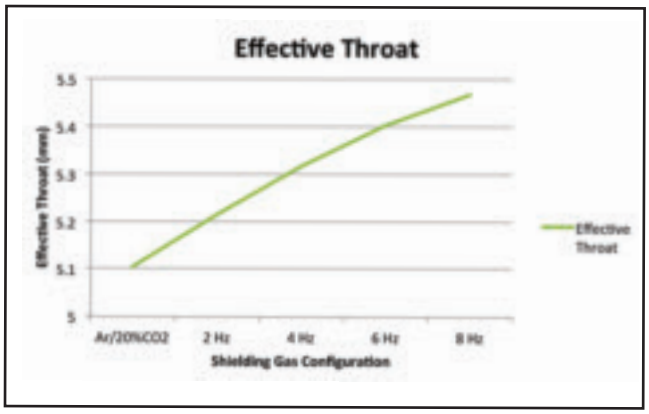

Fig. 10 — Effect of shielding gas configuration on predicted effective throat.

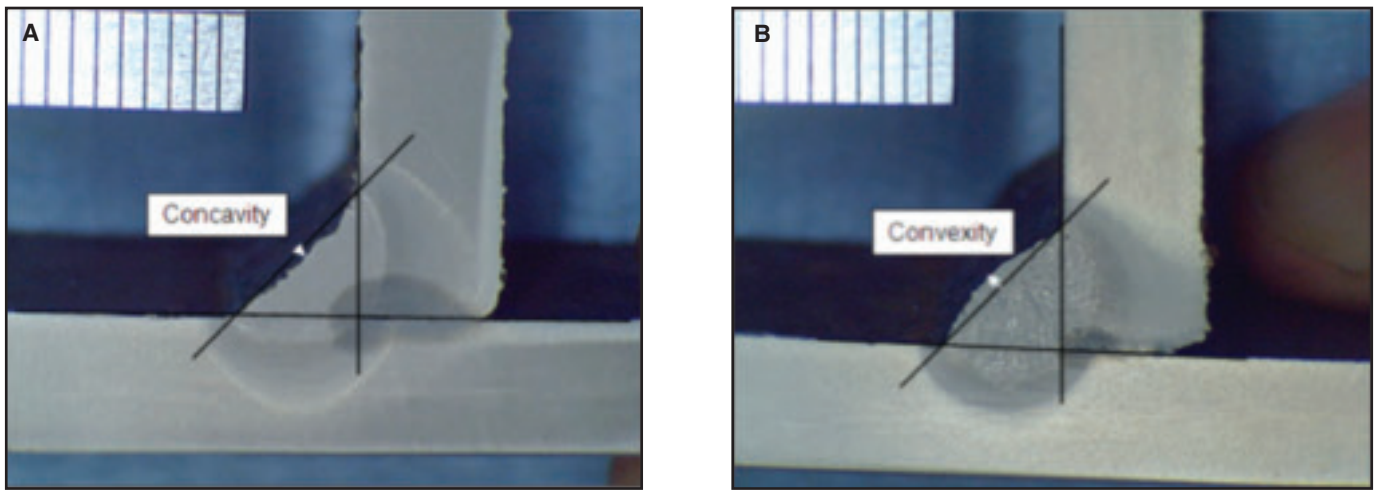

Fig. 11 — A — Weld profile showing the concavity of a typical weld produced using Ar/20%CO_2; B — weld profile showing the convexity of a typical weld produced using alternating shielding gases.

after the presentation of the entire training set. It was found that batch learning updates returned the lowest final error.

After this procedure, it was determined that the following network architecture provides the best-fitting model:

- Model Topology Multilayer Perceptron
- Iterations 8000
- Hidden Layers 1
- Momentum Coefficient 0.7
- Weight Updating Batch

The model, constructed according to the network architecture specified previously, was then validated against experimental data (Table 2B) not contained within the training or testing data. This was used solely to ensure the model was learning the trends among the training data, with the testing data being used for comparison in the later discussions.

Prediction of Weld Geometry

The model generated has been shown to accurately represent the weld penetration, leg length, and effective throat thickness by comparing the actual values with those predicted by the *NeuroSolutions* package as shown in Fig. 6. The software has been shown, on average, to overestimate weld penetration by 0.06 mm and underestimate leg length and effective throat thickness by 0.23 and 0.52 mm, respectively. When compared with the experimental data, this equates to percentage errors of 4.9, 3.4, and 9.6%, respectively, which is deemed as highly accurate in any ANN study.

The trained model was then applied to a given set of input parameters with the only variable being the shielding gas composition. The results (Fig. 7) show that the addition of helium has resulted in an increase in penetration, due to the narrower, more concentrated arc column that helium produces (Ref. 34), as depicted in Fig. 8.

Additionally, the prediction has shown that increasing the frequency of shielding gas alternation from 2 to 8 Hz resulted in a 0.03-mm increase in penetration. As a consequence, for a given level of penetration, the travel speed can be increased reducing the cost of the weld. It has been determined that for an equivalent level of penetration, the travel speed for alternating shielding gases can be increased, on average, by 28% over the Ar/20%CO_2 base case, and therefore has the potential to greatly increase the productivity of the welding process. This confirms the findings of Campbell et al. (Ref. 1), which demonstrated that the travel speed can be increased by 18% on the second pass and 82% on the third pass, thus resulting in an overall time reduction of 22%.

It has been widely publicized that plate distortion is a function of heat input. It has been reported that lower heat input welding processes result in less heat-induced distortion (Refs. 1, 35). The decrease in heat input, which would be as a result of the increased travel speed used to produce the equivalent levels of penetration when using alternating shielding gases, will also have beneficial effects with regard to weld-induced distortion.

The model has also shown that the application of alternating shielding gases results in a shorter leg length (Fig. 9), thus confirming the experimental results and is a consequence of the concentrated arc column that helium produces (Ref. 34). The effective throat thickness is shown to increase with the use of alternating shielding

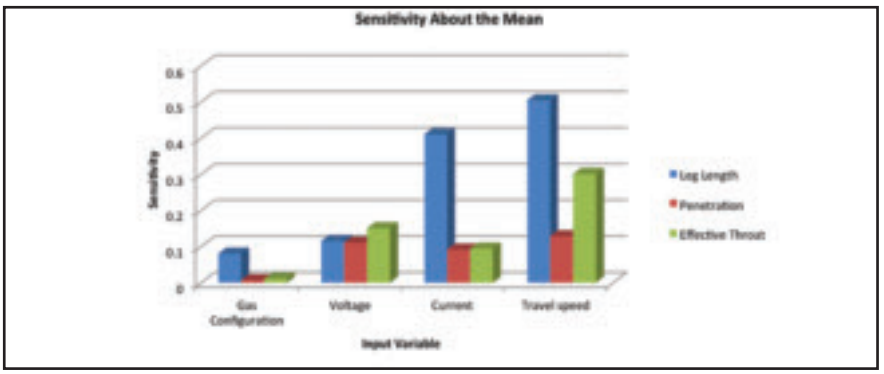

Fig. 12 — Sensitivity analysis results.

gases (Fig. 10); this is primarily linked to the added convexity of the weld metal with the addition of helium.

The macro images (Fig. 11) show that a typical alternating shielding gas weld produces a narrower weld with increased convexity (while Fig. 3 shows the measured dimensions). This, along with the results generated by the ANN model, show there is a trend between the shielding gas and the weld geometry. As reported by Kang et al. (Ref. 3), alternating shielding gases creates complex flow vectors within the molten weld pool, whereas constant gas flows produce a steady flow vector. It was reported that helium produces a flow vector that circulates inward, which will result in a narrower, more convex, weld profile. This is most probably due to the Marangoni effect in that the shielding gas configuration affects the surface tension of the weld, resulting in a thermocapillary convection phenomenon. As the Marangoni effect is governed by the temperature gradient on the weld pool surface and the temperature coefficient of the surface tension, it follows that, as helium has a higher arc power density than argon, it consequently produces a smaller cathode spot, an increased electromagnetic force, and an increase in the temperature gradient of the weld pool surface. Consequently, helium will have a greater Marangoni effect than argon and will thus create greater surface tension, which explains the narrower weld with greater penetration shown in Fig. 11.

Sensitivity Study

A sensitivity study is an extremely powerful tool in the *NeuroSolutions* package that can be used to determine the influence of each of the input variables on the output of the model.

In order to perform the sensitivity analysis, the neural network must first be trained as normal. The analysis then perturbs each of the inputs, one at a time, by a known variance from the mean while keeping all other variables at their respective means and measuring the change in the output.

The sensitivity for the input k can be expressed as shown in Equation 3.

$$S_k = \frac{\sum_{p=1}^{P}\sum_{i=1}^{o}\left(y_{ip} - \bar{y}_{ip}\right)^2}{\sigma_k^2} \qquad (3)$$

where S_k is the sensitivity for input k, $\bar{y}_{ip}$ is the i^{th} output obtained with the weights fixed for the, p^{th} pattern, o is the number of network outputs, p is the number of patterns, and σ^2_k is the variance of the input perturbation.

This, when applied across the training data, can compute how much a change in the input affects the output. The sensitivity of a model is not only important in the context of this model, i.e., determining the key factors for weld penetration, etc., but also aids the training of the model with inputs of high sensitivities having more importance in the mapping.

Sensitivity of Results

The results of the sensitivity study, Fig. 12, show that the travel speed is the most influential input variable in affecting the output variables. This is to be somewhat expected since the heat input, Q, is directly related to the travel speed through Equation 4.

$$Q = \frac{V * I}{1000 * TS} * \delta \qquad (4)$$

where V is the voltage (V), I is the current (A), δ is the thermal efficiency factor, and TS is the travel speed (mm/s).

The sensitivity study results show that the shielding gas configurations have the lowest contribution of the inputs on the weld geometries. However, this cannot be taken at face value and is a result of the sensitivity study perturbing the alternating frequency, e.g., comparing an alternating frequency of 5.9 Hz with 6 Hz. As can be seen in Figs. 6, 8, and 9, although there is a slight change in the geometries using different frequencies of alternation, the greatest step change is observed between the use of premixed Ar/20%CO_2 and alternating at 8 Hz; although, in fact, any frequency of alternation provides a similar step change. Figures 6, 8, and 9 also show that alternating shielding gases have a positive effect on the level of weld penetration while also reducing leg length and increasing the effective throat thickness.

Conclusions

A comparison of experimental and predicted results show that ANN software can be successfully employed to generate a model to predict multiple weld geometries. The results of the sensitivity analysis were in agreement with both findings of the experimental investigations and findings in other literature.

The ANN model has shown the ability to accurately identify subtle differences in the weld geometry, and has consequently produced a relationship linking the frequency of alternation to the weld penetration that has not previously been recognized. In doing so, this has shown that there is an inherent relationship between the frequency of alternation and the travel speed.

It has also been found that by training the model in reverse, the model can be implemented to determine the weld parameters required to produce a weld of specified geometry. The implementation of an ANN model for the prediction of the weld parameters necessary to satisfy a given geometry requirement can reduce the time required compared to determining the parameters experimentally, producing a noticeable economic benefit.

As a consequence of computational models becoming ever more advanced, their ability to accurately predict key weld geometries for a given set of parameters will help increase confidence that the resultant weld will be of this desired quality.

Acknowledgments

The authors would like to acknowledge the funding provided by BAE Systems Surface Ships Ltd., which made this research possible. Additional thanks are due to Dr. Martyn Lightfoot of the Shipbuilders and Shiprepairers Association and Simon Beckett of BAE Systems for their support.

References

1. Campbell, S. W., Galloway, A. M., and McPherson, N. A. 2011. Techno-economic evaluation on the effects of alternating shielding

gases for advanced joining processes. *Proceedings of IMechE Part B: Journal of Engineering Manufacture*, 225(8):1863–1872.

2. Chang, Y. H. 2006. Improve GMAW and GTAW with alternating shield gases. *Welding Journal* 85(2): 41–43.

3. Kang, B. Y., Yarlagadda, K. D. V. P., Kang, M. J., Kim, H. J., and Kim, I. S. 2009. Characteristics of alternate supply of shielding gas in aluminium GMA welding. *Journal of Materials Processing Technology* 209: pp. 4716–4121.

4. Kang, B. Y., Yarlagadda, K. D. V. P., Kang, M. J., Kim, H. J., and Kim, I. S. 2009. The effect of alternate supply of shielding gases in austenite stainless steel GTA welding. *Journal of Materials Processing Technology* 209: pp. 4722–4127.

5. Marya, M., Edwards, G. R., and Liu, S. 2004. An investigation on the effects of gases in GTA welding of a wrought AZ80 magnesium alloy. *Welding Journal* 83(7): 203-s to 212-s.

6. Tani, G., Campana, G., Fortunato, A., and Ascari, A. 2007. The influence of shielding gas in hybrid laser-MIG welding. *Applied Surface Science*, 253: pp. 8050–8053.

7. Galloway, A. M., McPherson, N. A., and Baker, T. N. 2011. An evaluation of weld metal nitrogen retention and properties in 316LN austenitic stainless steel. *Journal of Materials: Design and Applications* 225(2):61–69.

8. Jeffus, L. F. 2002. *Welding: Principles and Applications.* Cengage Learning, pp. 253–255.

9. *ASM Metals Handbook,* 8th Edition, Vol. 6, Welding and Brazing, p. 85. Materials Park, Ohio: ASM International.

10. McPherson, N. 2010. Correcting thin-plate distortion in shipbuilding. *Welding Journal* 89(1): 30–34.

11. Deng, D., and Murakawa, H. 2008. Prediction of welding distortion and residual stress in a thin plate butt-welded joint. *Computational Materials Science,* 43(2008): pp. 353–365.

12. Hong, L., and Ren, H. 2006. Simulation of welding deformations of ship structures. *Key Engineering Materials,* 324–325: pp. 651–654.

13. Lightfoot, M. P. 2008. Prediction of weld distortion using artificial neural networks. PhD thesis. University of Newcastle.

14. Principe, J. C., Euliano, N. R., and Lefebvre, W. C. 2000. *Neural and Adaptive Systems: Fundamentals through Simulations.* John Wiley & Sons, Inc.

15. McCulloch, W. S., and Pitts, W. 1943. A logical calculus of the ideas immanent in nervous activity. *Bulletin of Mathematical Biophysics* 5: pp. 115–133.

16. Rosenblatt, F. 1958. The perceptron: A probabilistic model for information storage and organization in the brain. *Psychological Review* 65(6): 386–408.

17. Widrow, B., and Hoff, M. E. 1960. Adaptive switching circuits. *IRE Wescon Convention Record*, Part 4, New York: IRE: pp. 96–104.

18. Werbos, P. J. 1974. Beyond regression: New tools for prediction and analysis in the behavioral sciences. PhD thesis, Harvard University.

19. Dornfeld, D. A., Tomizuka, M., and Langari, G. 1982. Modeling and adaptive control of arc welding processes. ASME Special Publication: *Measurement and Control for Batch Manufacturing*, November.

20. McGlone, J. C. 1982. Weld bead geometry prediction — A review. *Metal Construction* 14(7): 378–384.

21. Sterjovski, Z., Nolan, D., Carpenter, K. R., Dunne, D. P., and Norrish, J. 2005. Artificial neural networks for modelling the mechanical properties of steels in various applications. *Journal of Materials Processing Technology* 170: pp. 536–544.

22. Pal, S., Pal, S. K., and Samantaray, A. K. 2008. Artificial neural network modeling of weld joint strength prediction of a pulsed metal inert gas welding process using arc signals. *Journal of Materials Processing Technology*, 202: pp. 464–474.

23. Lakshminarayanan, A. K., and Balasubramanian, V. 2009. Comparison of RSM with ANN in predicting tensile strength of friction stir welded AA7039 aluminum alloy joints. *Transactions of Nonferrous Metals Society of China*, 19: pp. 9–18.

24. Reddya, N. S., Krishnaiahb, J., Hong, S., and Lee, J. S. 2009. Modeling medium carbon steels by using artificial neural networks. *Materials Science and Engineering A*, 508: pp. 93–105.

25. Ates, H. 2007. Prediction of gas metal arc welding parameters based on artificial neural networks. *Materials and Design* 28: pp. 2015–2023.

26. Pal, S., Pal, S. K., and Samantaray, A. K. 2010. Prediction of the quality of pulsed metal inert gas welding using statistical parameters of arc signals in artificial neural network. *International Journal of Computer Integrated Manufacturing* Vol. 23, No. 5, pp. 453–465.

27. Lightfoot, M. P., Bruce, G. J., McPherson, N. A., and Woods, K. 2005. The application of artificial neural networks to weld-induced deformation in ship plate. *Welding Journal* 84(2); 23-s to 26-s.

28. Lightfoot, M. P., McPherson, N. A., Woods, K., and Bruce, G. J. 2006. Artificial neural networks as an aid to steel plate distortion reduction. *Journal of Materials Processing Technology*, 172: pp. 238–242.

29. Nagesh, D. S., and Datta, G. L. 2008. Modeling of fillet welded joint of GMAW process: Integrated approach using DOE, ANN, and GA. *Int J Interact Des Manuf*, 2: pp. 127–136.

30. Nagesh, D. S., and Datta, G. L. 2010. Genetic algorithm for optimization of welding variables for height to width ratio and application of ANN for prediction of bead geometry for TIG welding process. *Applied Soft Computing*, 10: pp. 897–907.

31. Beckett, S., MacPherson, M. J., and McPherson, N. A. 2011. Improved welding control of automated fillet welding for ship structures using artificial neural networks (ANN). Presented at JOM 16 Conference, May 2011, Helsingør, Denmark.

32. Zeng, X. M., Lucas, J., and Fang, M. T. C. 1993. Use of neural networks for parameter prediction and quality inspection. *Transactions of the Institute of Measurement and Control* 15(2): pp. 87–95.

33. Anderson, K., Cook, G. E., Ramaswamy, K., and Karsai, G. 1990. A novel approach towards relationships between process variables and weld geometry. *Recent Trends in Welding Science Technology*, May 1989, Gatlinburg, Tenn., pp. 997–1003.

34. Jönsson, P. G., Eagar, T. W., and Szekely, J. 1995. Heat and metal transfer in gas metal arc welding using argon and helium. *Metallurgical and Materials Transactions B* 26B: pp. 383–395.

35. Deng, D., and Murakawa, H. 2008. FEM prediction of buckling distortion induced by welding in thin plate panel structures. *Computational Materials Science*, 43: pp. 591–607.

AWS Debuts Careers in Welding Trailer

The AWS Careers in Welding Trailer offers many attractive features to get young people excited about welding industry careers.

In particular, the mobile exhibit showcases the following:

- Five of The Lincoln Electric Co.'s VRTEX® 360 welding simulators that feed computer-generated data with a virtual welding gun and helmet equipped with internal monitors;
- Interactive educational exhibits, including a display wall featuring 11 industry segments with trivia questions, fun facts, and industry artifacts;
- "Day in the Life of a Welder" exhibit with videos depicting real-life environments in which welders work;
- Life-size welder highlighting welding as a safe profession;
- Social media kiosk; and
- Welding scholarship information.

The 53-ft, single expandable trailer designed and built by MRA experiential tours and equipment covers 650-sq-ft of exhibit space.

It is expected the trailer will be on the road for 18–24 weeks in 2012. To learn more and view its schedule, visit *www.explorewelding.com*.